Evaluation of the impact of local sensing data and feature extraction techniques on high frequency intra-hour irradiance forecasting

Erling W. Eriksen, Heine N. Riise, Magnus M. Nygård

(Dated: February 9, 2024)

SUMMARY OF THE ABSTRACT

An investigation and evaluation of feature extraction and modelling methodologies for intra-hour forecasting using two All Sky Imagers (ASI) for a 22.6 kW PV System owned and operated by the Institute of Energy technology, Kjeller, Norway. Several feature extraction methods were applied, along with different machine learning forecasting techniques on the 1 Hz irradiance and 0.1 Hz image data to investigate the flow of information from data to prediction. From the ASI images, a Cloud Motion Vector (CMV), cloud segmentation and Cloud Base Height (CBH) was extracted, constituting a set of exogenous features for irradiance forecasting. These features were used to construct an initial baseline model, a two-layer LSTM network with a vector output, which achieved an Mean Sqwuared Error (MSE) Skill Score (SS) exceeding 0.3 against a simple persistance model.

EXPLANATORY PAGES

A. Introduction

As a result of the increasing integration of renewables in the electricity grid, intermittent, variable power sources have an increasing share in the energy market. With this, short term, intra-hour forecasts have gained increased usefulness for grid regulation and cost mitigation [1]. Additionally, off-grid operations requiring stable power sources, with limited compensation strategies for the variability of insolation, may gain from efficient utilization of short-term forecasting in their control strategies by predicting large, sudden changes in power, called ramp events [2].

There are many proposed methodologies for intra-hour forecasting, but they are rarely benchmarked against each other [3][1]. The development of novel forecasting techniques is also closely tied to development in machine learning, where time series prediction is a major area of research. The use of high-frequency local sensing techniques has emerged as the most successful forecasting method and at this point the scope of possible solutions within this space is vast[1]. Of particular focus in recent exploration are Long Short-Term Memory (LSTM) recurrent Neural Networks (RNN), that have been proposed in a wide array of forecasting models [4][5][6][7][8].

Each choice of method affects the information pathway from source data to prediction, affecting the signal to noise ratio. This is especially true for local sensing techniques since they depend on extracting useful local information for the relevant site. As the main factor for intra-hour forecast performance is attenuation of irradiance through cloud presence, movement and shade casting, the feature extraction from All Sky Imager (ASI) images must detect and preserve this information for input into predictive algorithms. The simpler the relation between the input and target variables, the easier it is for models to find the relevant pattern for prediction. Therefore, feature extraction that preserves and simplifies patterns in the data is essential for building efficient models. Additionally, for dense data, like images in time series, feature extraction can reduce necessary computation time, which is important for real time applications.

Some work propose extracting information in a way which enables a 3D spatial model to be built from the ASI images, which can be propagated to create a probabilistic forecast[9]. Others, like S. Song et. al. and X. Feng et. al. rely on black box Convolutional Neural Netorks(CNN) to intuitively extract useful features. [10][11].

Extracting features gives insight into the flow of information of the model, by what information it can successfully use to predict patterns. Do features built on a physical understanding of the atmosphere perform better because they describe an important relationship or is there information present in these data sources that is best captured by using black-box feature extractors like CNN's or latent encoders? Is the usefulness of each feature extraction method dependent on what model one chooses? Investigating this landscape of different feature extraction methods and models as well as their interactions is essential for progressing the field and ultimately developing better forecasts while avoiding dead ends that have already explored.

B. Methodology

1. *Data acquisition*

Data was gathered from two ASIs (ASI A and ASI B) positioned at 59.95 °N latitude, separated by 1.6

km. Images were captured every 10 seconds over a period of 1.5 years from July 2022 to December 2023. Between the two ASIs there is a $22.6kW_p$ PV system owned and operated by the Institute for Energy Technology (IFE). For the preliminary exploration, a single day, August 6th 2022, was selected for its relatively long nordic daylight duration and the presence of scattered multilayered clouds throughout the day, as can be seen in Figure 1. Thus, the day exhibits varied cloud conditions that are known to be challenging to forecast.

2. Image processing

To determine the orientation of the skycameras in relation to each other, the images were rotated to align along a North-South axis. This was done by finding the sun in each image for 7 clearsky days between February 2023 and September 2023 using a linear threshold for brightness along with a center of mass algorithm implemented in version 1.11.1 of the python package `SciPy`. This enabled us to find the central location within the sun-area [12]. The solar position in the images was then compared to the solar position calculated using functionality implemented in version 0.10.1 of the python package `pvlib`[13]. The discrepancy between the suns azimuth value was used as the azimuthal offset of each camera.

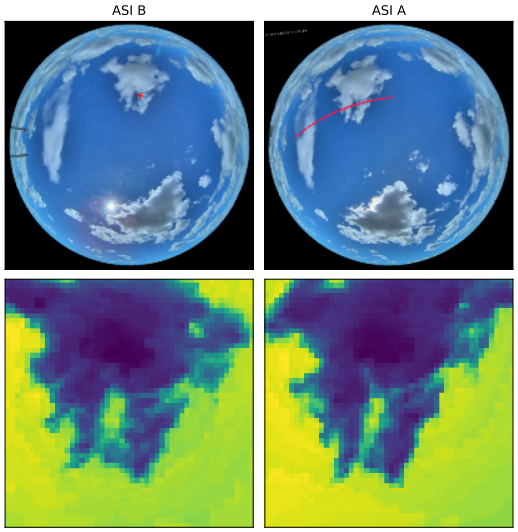

Figure 1: In the top right image, an epipolar line in red is plotted corresponding to selected pixel marked with a red cross in the top left. In the lower images, the pixel match area for two ASI images taken by different cameras at the same time. The match is done on the saturation of the image, where in these images a lighter, more yellow color indicates a higher saturation, while a darker, bluer color indicates a lower saturation.

To account for the distortion of the zenith in each camera, as caused by the geometry of the fisheye lens, a reverse image projection was used to project the fisheye image to a flat plane. The lenses used had an equidistant geometry, described by

$$\theta_{pixel}/\theta_{FOV} = r_{pixel}/R_{img} \tag{1}$$

where θ_{pixel} and r_{pixel} are the zenith angle and image radius of each pixel, R_{img} is the total image radius and θ_{FOV} is the zenith of the camera field of view (FOV). Additionally, real lens geometries deviate from the mathematical description, and so a table of deviations from Equation (1) was received from the producers of the ASI, and used to create a 7th order polynomial fit describing the deviations. This polynomial was then used in addition to Equation (1) to transfer between the radius of each pixel in the raw sky-images and its zenith angle.

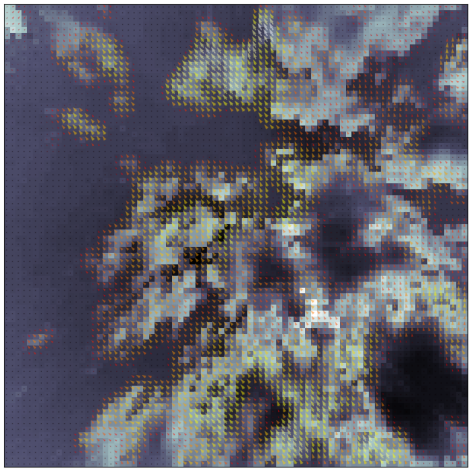

Figure 2: Cloud movement vector between consecutive images, illustrated by arrows pointing in the direction of movement and the color indicating the magnitude of the velocity

3. Feature Extraction

To classify cloud pixels in each ASI image, K Nearest Neighbour (KNN) clustering was performed in the RGB color space [14]. The clusters were classified using comparisons of mean saturation, under the assumption that the statistics of the clusters are more separable than those of the individual pixels. The speed of this method was increased by application of principle component analysis (PCA) decomposition, compressing the RGB color space into two dimensions [15].

Using pairs of subsequent ASI images, motion can be extracted for each pixel using dense optical flow.

The Cloud Motion Vector (CMV) was estimated numerically using the Farnebäck Optical flow methods included in the python library `OpenCV 4.8.0` [16][17]. An example of an extraction can be seen in Figure 2.

As proposed by D. Nguyen and J. Kleissl, the cloud base height was estimated using epipolar geometry [3]. In this algorithm, each point in an image captured by ASI B has an epipolar line constituting it's possible positions in the corresponding image captured by ASI A. This relationship is highlighted in the upper two images of Figure 1. Finding a matching window, as shown in the lower two plots of Figure 1 around the point and along the epipolar line, determines the CBH of the point [3]. This can be repeated for all pixels classified as clouds, to extract a matrix of CBHs.

4. Modelling

A series of features extracted by application of the methods described in section were used to build an LSTM model with varying features to assess the utility of local exogenous features. The selected network for the comparison in this work contained two LSTM layers with 30 neurons each. A dropout layer was included between the recurrent layers to reduce overfitting, with a dropout rate of 10%. Moreover, a dense layer was added as the last layer, with a number of neurons corresponding to the prediction horizon.

Global Horizontal Irradiance (GHI) data measured with a Kipp & Zonen SMP10 Pyranometer of 1Hz frequency was scaled to a range between 0 and 1 and split into a training, validation and test set as shown in the upper panel of Figure 3. NaN values were filled with the closest previous value avoiding information leak backwards in time, while the GHI data was resampled to the frequency of the ASI images (0.1 Hz) using the mean. The models were validated using walk-forward validation, only training on past data, and predicting on future unseen data [18].

Evaluations of the forecast performance was done with the Mean Squared Error (MSE),

$$MSE = \sum_{i=0}^{n} \frac{(y_i - \hat{y}_i)^2}{n} \tag{2}$$

where y_i is the true irradiance value, $\hat{y}_i$ is the forecasted irradiance value and n is the number of timesteps in the forecast and the MSE Skill Score (SS), defined as

$$SS = 1 - \frac{MSE_f}{MSE_{ref}} \tag{3}$$

where MSE_f and MSE_{ref} is the MSE of the forecast and reference model, respectively. In the present work, the reference was a persistance model, this simple model assumes that the irradiance will remain constant to the last know irradiance was used as a reference model.

C. Results and Conclusion

1. Feature extraction

Features were extracted for the 6th of August 2022 for a period period between 8:30 and 17:00. The period in question contains scattered multilayered clouds with scattered cumulus cloud as well as higher altocumulus clouds as shown in the ASI images of Figure 1. Each image resulted in feature maps corresponding to velocities in the x- and y-direction, a cloud mask and an single estimate of CBH for ASI

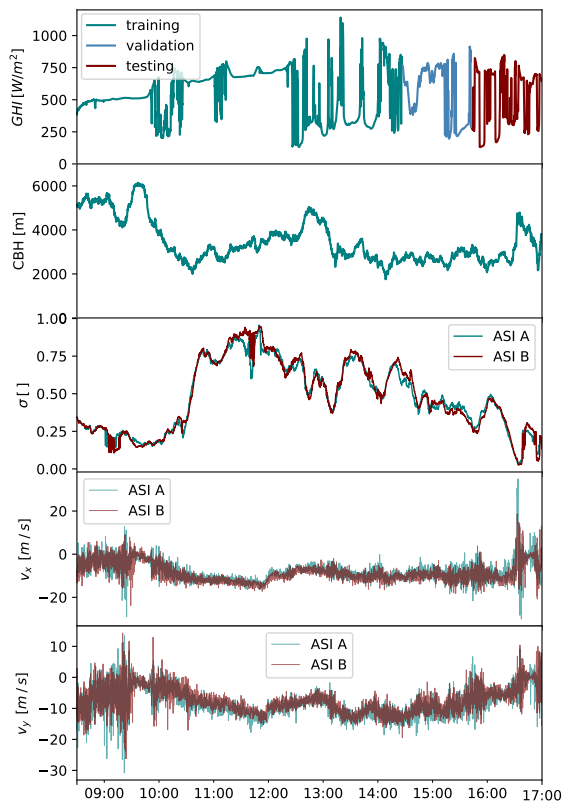

Figure 3: GHI and extracted features between 08:30 and 17:00 on the 6th of August. ASI A and ASI B refer to the two skycameras positioned 1.6 km apart. GHI data for the day is also split into subsets of the LSTM training, validation and testing.

A. These maps were then aggregated using the mean, resulting in the time series presented in Figure 3.

The cloud speed estimates correspond with a direction matching what can be determined by observation, but exhibit significant oscillations. This may be due to propagation of uncertainty from the cloud mask, as well as the effect of aggregation from a complete map of velocities into a mean. A step to improve this is to calculate the velocities from higher resolution images, which are available, but requires a more time-consuming computation.

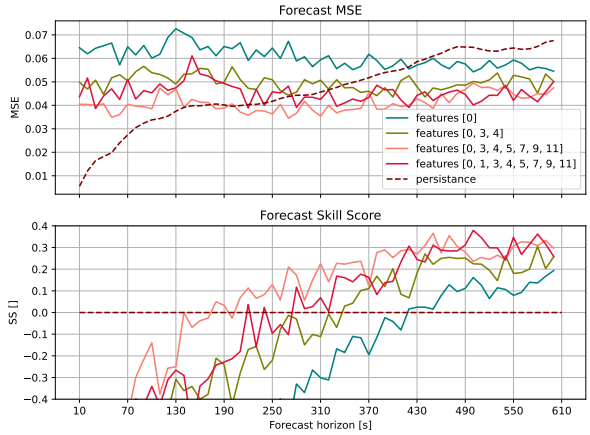

Figure 4: LSTM prediction on test set using different features for a forecasting horizon up to 10 min, with a lookback of 5 min.

2. *Predictive modelling*

The results presented in Figure 4 demonstrate that a persistence forecast outperforms the current LSTM forecast for very short time-horizons. However for longer horizons than 200 s, the LSTM model achieves positive skill scores. The LSTM model gains accuracy with the addition of exogenous features described in Table I, this is especially the case for longer time horizons.

Utilizing local data sources in the best way is challenging, and not often discussed thoroughly in the literature. For this preliminary work, features related to physical observables have been extracted, and used as inputs. in the next step of the present work, we will compare these features to others extracted by black-box methods as well as spatially resolved features. The forecasting work so far agrees with the literature in that it shows image extraction from ASI images and their utility in forecasting, although using more data and an expanded set of models and features will yield a more thorough understanding. The use of an LSTM networks on irradiance and image features, shows that for a small 8 hour dataset, without any hyperparameter optimization or network structure optimization, an LSTM outperforms a persistance forecast for and is aided further by local extracted features.

Table I: Table of exogenous features with accompanying number used in Figure 4

Feature	Feature number
GHI	0
CBH	1
Cloudiness ASI A	3
Cloudiness ASI B	4
v_x ASI A	5
v_y ASI A	9
v_x ASI B	7
v_y ASI B	11

[1] Y. C. et al., iScience **24**, 103136 (2021).
[2] S.-A. L. et al., Renewable Energy **199**, 246 (2022).
[3] D. A. N. et al., Solar Energy **107**, 495 (2014).
[4] S. H. et al., Neural computation **9**, 1735 (1997).
[5] Y. W. et al., Sustainability **13** (2021).
[6] N. L. M. J. et al., Processes **11** (2023).
[7] H. C. et al., Energy Reports **7**, 1047 (2021), 2021 International Conference on Energy Engineering and Power Systems.
[8] J. S. et al., Energy Science & Engineering **10**, 2909 (2022).
[9] B. N. et al., Solar Energy **253**, 285 (2023).
[10] S. S. et al., Energy Reports **8**, 125 (2022), iCPE 2021 - The 2nd International Conference on Power Engineering.
[11] C. F. et al., Applied Energy **310**, 118438 (2022).
[12] P. V. et al., Nature Methods **17**, 261 (2020).
[13] W. F. H. et al., Journal of Open Source Software **3**, 884 (2018).
[14] J. M. et al., in *Proceedings of the fifth Berkeley symposium on mathematical statistics and probability*, Vol. 1 (Oakland, CA, USA, 1967) pp. 281–297.
[15] K. P. F.R.S., The London, Edinburgh, and Dublin Philosophical Magazine and Journal of Science **2**, 559 (1901).
[16] Itseez, "Open source computer vision library," `https://github.com/itseez/opencv` (2015).
[17] G. Farnebäck (2003) pp. 363–370.
[18] R. E. Pardo, *Design, Testing and Optimization of Trading Systems*, 1st ed. (J. Wiley., 1992) p. 108–119.